

트리에틸렌 글리콜 치환된 합금속 나프탈로시아닌의 합성과 근적외 흡수 특성 연구

한성훈* · 고팔 발라무루간* · 장재웅* · 손범용* · 팜티누구엣* · 이승걸**** · 박종승****,†^{ORCID}

*부산대학교 응용화학공학부, **부산대학교 유기소재시스템공학과
(2021년 6월 25일 접수, 2021년 7월 22일 수정, 2021년 7월 23일 채택)

Synthesis and NIR Absorption Properties of Triethylene Glycol Substituted Metallo-Naphthalocyanines

Seong-Hun Han*, Gopal Balamurugan*, Jae Woong Jang*, Fayong Sun*,
Nguyet N. T. Pham*, Seung Geol Lee****, and Jong S. Park****,†^{ORCID}

*School of Chemical Engineering, Pusan National University, Busan 46241, Korea

**Department of Organic Material Science and Engineering, Pusan National University, Busan 46241, Korea

(Received June 25, 2021; Revised July 22, 2021; Accepted July 23, 2021)

초록: 다양한 전이 금속의 존재하에서 트리에틸렌 글리콜(TEG) 치환체를 가지는 합금속 나프탈로시아닌 유도체(MNPs)를 합성하고, 이들의 광학적 및 근적외(NIR) 영역에서 흡수 특성을 조사하였다. UV-Vis 스펙트럼 측정 결과에 따르면 MNPs는 나프탈로시아닌 구조 주변부에 부가된 페닐링과 비주변부(non-peripheral) 위치에 치환된 전자주게 치환체로 인해 NIR 영역에서 강한 흡수 특성을 나타내었다. 또한, MNPs의 최대 흡수파장은 중앙부 금속의 종류에 따라 780에서 950 nm까지 광범위하게 조정할 수 있었다. 또한, 친수성이 강한 TEG 치환체가 존재함에 따라 극성 용매에서의 용해도와 고분자 매트릭스에 대한 상용성이 크게 증진하는 효과를 나타내었다. 높은 NIR 영역 흡수 및 가시광 투과도를 보이는 MNPs의 특성을 이용하여 근적외 차단 필름을 제조하였다. 니켈-나프탈로시아닌(nickel naphthalocyanine)을 포함하여 근적외 차단 필름을 제조하였을 때 안티몬 주석 산화물(ATO) 단독 대비 가시광선 투과성은 그대로 유지하면서 근적외 차단 성능을 향상할 수 있는 것으로 확인되었다. 상기 결과로 보건데 근적외 차단 물질로서의 합금속 나프탈로시아닌의 효능을 확인할 수 있으며, 이는 근적외 흡수성과 극성 매체에 대해 상용성을 동시에 발휘하는 것에 기인하는 것이다.

Abstract: Naphthalonitrile substituted with triethylene glycol (TEG) in the presence of transition metals synthesized a series of metallo-naphthalocyanine derivatives (MNPs), and it was investigated that the optical and near-infrared (NIR) absorption properties. In UV-Vis spectra measurements, these MNPs exhibited strong absorption in the NIR regions because of the annulated benzene ring of naphthalocyanine and highly electron-donating substituents attached at the non-peripheral positions. The absorption wavelength of MNPs was effectively adjusted in NIR ranges from 780 to 950 nm by inserting various central metals. Additionally, the presence of TEG-substituents in MNPs significantly enhanced the solubility in highly polar solvents and the compatibility with the polymer matrix. NIR blocking films were fabricated for taking advantage of high NIR absorption and visible transmittance. When NIR film was fabricated with nickel-naphthalocyanine, it was confirmed that the NIR cutting property can be improved while maintaining the visible light transmittance compared to the antimony tin oxide (ATO). From the observations, the feasibility of designed MNPs as an effective NIR blocking material was evidenced, which is attributed to its strong NIR absorption and compatibility in the polar mediums.

Keywords: naphthalocyanine, triethylene glycol, near-infrared blocking film, near-infrared filter.

Introduction

Excessive solar heat consumes extra energy to maintain

internal temperatures and adversely affects environmental issues. Near-infrared (NIR) rays, ranging from 700 to 3000 nm, constitute ~52% of the total solar energy.¹ The majority of the solar power is located in the radiation between 700 and 1200 nm. The NIR rays have been known for increasing the internal temperature.² More energy consumption tends to be used in maintaining a constant internal temperature of the

†To whom correspondence should be addressed.
jongpark@pusan.ac.kr, ORCID[®]0000-0002-7624-9502
©2021 The Polymer Society of Korea. All rights reserved.

buildings. Thus, NIR barriers have been developed to prevent NIR rays from entering the buildings. Active research is still going with various metal oxides as NIR blocking materials.³⁻⁵ Antimony tin oxide is inexpensive among metal oxides, and has a transmittance of over 70% in the visible light region, and has been used as heat-shielding material for NIR blocking.⁶⁻⁸ But, ATO has the disadvantage of having a relatively low cut-off in the NIR region between 700 and 1000 nm.⁹ The combination with organic dyes was found helpful in improving the NIR blocking but often caused the large aggregates due to the reduced solubility.

Phthalocyanines (Pcs) are well-known macrocyclic pigments with good thermal and chemical stability.¹⁰ Pcs exhibited characteristic dual absorption spectra, showing a Q-band in 600-700 nm and a B-band in 300-400 nm, with the coverage of green and blue colors.¹¹ Meanwhile, naphthalocyanine (NPc) is a cyclotetramerized product of naphthalonitrile whose π -system is further expanded by fused benzene rings. The extended π -electrons of NPcs induce a significant red shift in Q-band absorption, compared to that of Pc.¹² The substituents of the electron-rich groups at the non-peripheral positions destabilized the highest occupied molecular orbital (HOMO) state of Pc, resulting in the substantial red-shift of the Q-band to the NIR region.^{13,14} Similarly, it is expected that the non-peripheral functionalization of NPc facilitates the red-shift of the Q-band. Therefore, NPcs showing strong absorption at NIR regions can be a potential candidate in organic solar cells, photodynamic therapy, heat absorbers, and NIR imaging.¹⁴⁻¹⁷ However, NPcs suffered from severe aggregation due to low solubility.¹⁸ In order to improve the solubility of NPcs, the non-peripheral substitution can be extended with long-chain substituents, preferentially having non-polar nature.

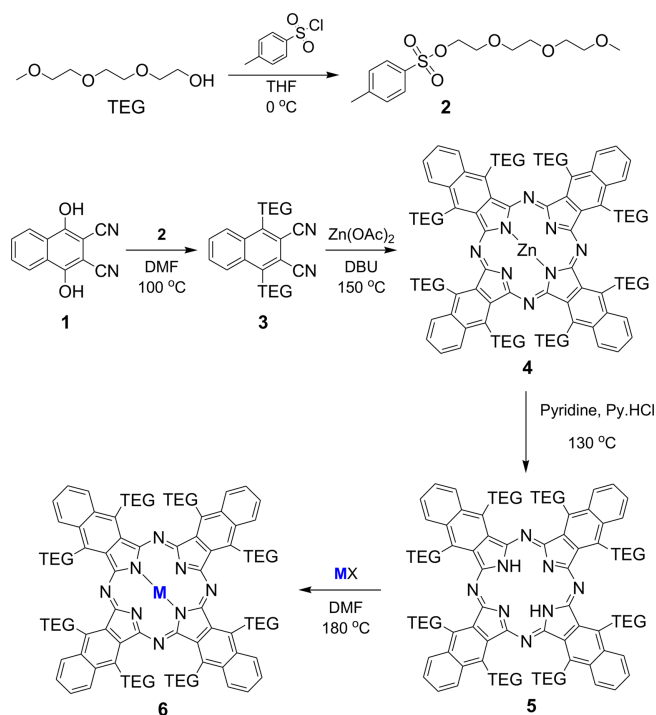
This article presents the preparation and applications of hydrophilic NIR absorbing metallo-naphthalocyanines (MNPcs). Various central metals, including Ru, Zn, Ni, and Sn, have been incorporated in the central position to fine-tune the Q-band, thus delicately modifying the absorption in NIR ranges. As far as we know, no previous reports have been made concerning the systematic investigation of MNPcs. In order to improve the solubility in common solvents and compatibility with the polymer matrix, trimethylene glycol (TEG) groups were selected and introduced at non-peripheral positions (TEG-MNPc). The optical properties of the prepared TEG-MNPc were examined depending on the inserted metals. The electrochemical properties of MNPcs were investigated in terms of cyclic voltammetry (CV) measurements. The nickel-

naphthalocyanines (NiNPc)-ATO hybrid mixture was prepared in the photocurable resin, and the NIR blocking efficiency was examined by measuring transmittance in the 380-2500 nm region.

Experimental

Chemicals and Materials. 2,3-Dichloro-1,4-naphthaloquinone, 1,8-diazabicyclo(5.4.0)undec-7-ene (DBU) was purchased from ThermoFisher (Korea). Triethylene glycol monomethyl ether and *p*-toluenesulfonyl chloride (*p*-TsCl) were purchased from TCI (Korea). Poly (vinylidene fluoride-co-hexafluoropropylene) (PVDF-HFP), 1-butyl-3-methylimidazolium (trifluoromethylsulfonyl)imide (BMIM-TFSI), potassium carbonate, sodium hydroxide, and metal chlorides (Zn, Ni, Sn, etc.) were purchased from Sigma Aldrich (Korea), and used as received. Solvents including *n*-butanol and ethanol were purchased from Daejung Chemicals (Korea). Indium tin oxide (ITO, 15 Ω) coated glass slides used as electrode substrates were obtained from Wooyang GMS (Korea). ATO solution (40 wt%, MIBK) and acrylic-based photocurable resin were provided by AMTE (Korea).

Synthetic Procedures. The overall synthetic procedures are represented in Scheme 1.



Scheme 1. Synthetic procedures of TEG-substituted metallo-naphthalocyanines (MNPcs).

Synthesis of 1,4-Dihydroxy-2,3-naphthalonitrile (1): 2,3-Dichloro-1,4-naphthaloquinone (9.0 g, 39.6 mmol) was dissolved in 150 mL of ethanol and stirred at room temperature. After that, sodium cyanide (12.0 g, 244.9 mmol) dissolved in distilled water (100 mL) was slowly added to the 2,3-dichloro-1,4-naphthaloquinone solution. During the addition, the temperature was maintained below 40 °C. After complete addition, the mixture was further stirred for 1 h at room temperature. HCl was added to the dark red solution. The solid present in mixture was then filtered, washed with water, and dried in an oven at 80 °C. Finally, a pale red product was obtained and used for the subsequent reaction without further purification.

Synthesis of Triethylene Glycol Monomethyl Ether Tosylate (TEG Tosylate) (2): Triethylene glycol monomethyl ether (16.4 g, 100 mmol) was dissolved in THF (100 mL), and sodium hydroxide (14 g, 350 mmol) dissolved in water was slowly added to THF solution. The mixture was cooled down below 5 °C in an ice bath. *p*-Toluenesulfonyl chloride (19 g, 100 mmol) in THF (50 mL) was added dropwise to the mixture in the ice bath. The mixture was stirred at 0 °C for 2 h and stirred at room temperature for 12 h. After that, 5 wt% aqueous hydrochloric acid solution was added. Then, the product was extracted with dichloromethane from the water layer. The dichloromethane layer was washed with sodium bicarbonate solution and distilled water, and then dried over anhydrous MgSO₄. The product was obtained as a colorless liquid by evaporating dichloromethane, and the yield was 92%. ¹H NMR (500 MHz, CDCl₃): 7.77 (d, 2H; Ar-H), 7.32 (d, 2H; Ar-H), 4.15 (t, 2H; CH₂), 3.68 (t, 2H; CH₂), 3.62-3.56 (m, 6H; CH₂), 3.53-3.50 (m, 2H; CH₂), 3.36 (s, 3H; CH₃), 2.44 (s, 3H; CH₃).

Synthesis of 1,4-DiTEG-2,3-naphthalonitrile (3): In a 250 mL round-bottom flask, 1,4-dihydroxy-2,3-naphthalonitrile (1) (3 g, 14.3 mmol), TEG tosylate (2) (11.3 g, 35.7 mmol), and K₂CO₃ (4.93 g, 35.7 mmol) were added to DMF (50 mL). The reaction mixture was stirred under an argon atmosphere at 90 °C for 24 h. DMF solvent was evaporated *in vacuo*, and water (100 mL) was poured into the residue, extracted three times with dichloromethane. The organic layer was dried over anhydrous MgSO₄. The product was purified by silica gel column chromatography using dichloromethane/methanol (25:1 v/v). The final product was obtained as a red oil. ¹H NMR (500 MHz, CDCl₃): 8.39 (q, 2H; Ar-H), 7.77 (q, 2H; Ar-H), 4.57 (t, 4H; CH₂), 3.95 (t, 4H; CH₂), 3.75-3.63 (m, 12H; CH₂), 3.55-3.52 (m, 4H; CH₂), 3.37 (s, 6H; CH₃).

Synthesis of Zinc Octa-TEG-naphthalocyanine (4): 1,4-diTEG-2,3-naphthalonitrile (3) (2000 mg, 4.0 mmol), zinc acetate (366.96 mg, 2.0 mmol), butanol (5 mL), and two drops of DBU were mixed in a pressure tube. The mixture was stirred at 150 °C for 12 h. After cooling to room temperature, the solvent is removed under vacuum, and the residue was extracted with dichloromethane (DCM). The extracted organic layer was dried over anhydrous MgSO₄, and the product was purified by ethyl acetate/methanol (20:1 v/v) silica gel column chromatography (0.68 g, yield: 32.8%). ¹H NMR (500 MHz, CDCl₃): 8.30 (q, 8H; Ar-H), 7.71 (q, 8H; Ar-H), 4.54 (t, 16H; CH₂), 3.92 (t, 16H; CH₂), 3.75-3.63 (m, 48H; CH₂), 3.53-3.50 (m, 16H; CH₂), 3.37 (s, 24H; CH₃). MALDI-Mass (C₁₀₄H₁₃₆N₈O₃₂Zn) 2074.850 m/z.

Synthesis of Metal-free Octa-TEG-naphthalocyanine (5): Zn-octa-TEG-naphthalocyanine (500 mg, 0.24 mmol) (4) and pyridine-HCl (5 g, excess) was mixed with pyridine (50 mL). The mixture was stirred at 130 °C for 17 h. After cooling to room temperature, the solvent is removed under vacuum, and the residue was extracted with distilled water and ethyl acetate. The extracted organic layer was dried over anhydrous MgSO₄, and the product was purified by ethyl acetate/methanol (20:1 v/v) silica gel column chromatography. (0.41 g, yield: 84.6%). ¹H NMR (500 MHz, CDCl₃): 8.31 (q, 8H; Ar-H), 7.85 (q, 2H; NH), 7.70 (q, 8H; Ar-H), 4.54 (t, 16H; CH₂), 3.92 (t, 16H; CH₂), 3.75-3.63 (m, 48H; CH₂), 3.53-3.50 (m, 16H; CH₂), 3.36 (s, 24H; CH₃). MALDI-Mass (C₁₀₄H₁₃₈N₈O₃₂) 2011.992 m/z.

General Procedure for the Synthesis of Metallo-octa-TEG-naphthalocyanine (6): Metal-free octa-TEG-naphthalocyanine (200 mg, 0.099 mmol) (5), metal salts (0.15 mmol), such as SnCl₂, NiCl₂, and Ru₃(CO)₁₂, in DMF (5 mL) was mixed in a pressure tube. The mixture was stirred at 130 °C for 3 h. After cooling to room temperature, the solvent was removed in a vacuum and washed by adding water and DCM to remove metal chloride. The extracted DCM layer was dried over anhydrous MgSO₄. The product was obtained by evaporation.

DFT Calculations. All calculations were performed with the Gaussian 09. The structure optimization and the bandgap energy levels calculation were executed at the B3LYP/6-31G level. The effective core potential has been employed by considering the outermost electrons and binding the rest into one core suitable for the electron-rich metal ions. In SnNPc and RuNPc calculations, the effective core potential with LanL2DZ (Los Alamos National Laboratory double zeta) was used.

Electrochemical Property. The MNPC ionic gels were prepared by mixing MNPCs (0.2 g), PVDF-HFP (0.8 g), BMIM-TFSI (3.2 g) in acetone (5 mL). The solution was stirred at 70 °C overnight to mix thoroughly. Then, the ionic gel was coated on ITO glass by drop-casting, and the Surlyn[®] was placed on the ITO glass to act as a spacer. After that, acetone was removed by placing it on a hot plate at 70 °C for 5 min. After the solvent was removed, another ITO glass is bonded in a sandwich form to complete the device. The fabricated electrochemical cells were used to evaluate the cyclic voltammetric properties of MNPCs.

Preparation of MNPC-based Infrared Blocking Films. The NiNPC-ATO hybrid mixture was prepared by mixing a photocurable resin, ATO, and NiNPC with a small amount of DCM (0.2 mL). The prepared solution was stirred at room temperature for 1 hour to mix thoroughly. The stirred solution was coated on a glass slide (7.5×2.5 cm²) with a thickness of 100 μm by a doctor blading method. After that, it was dried in an oven at 100 °C for 15 min to remove the solvent. Photocuring was carried out for 1 min with 144 mJ/cm² irradiation in a UV lamp chamber (365 nm).

Results and Discussion

The direct cyclotetramerization of TEG attached phthalonitrile using different metal salts, such as Zn(OAc)₂, SnCl₂, NiCl₂, and Ru₃(CO)₁₂, in the presence of DBU was initially carried out. Among other metal salts, zinc-naphthalocyanine, ZnNPC, was initially produced in a high yield. ZnNPC was easily converted by pyridinium hydrochloride to yield free NPC, which was subsequently used to make other MPc in a considerable yield. The presence of TEG substituents enhanced the solubility of NPCs in most of the polar solvents.

Table 1. Maximum Absorption Wavelength and Molar Extinction Coefficient of MNPCs

| MNPc | RuNPC | ZnNPC | NiNPC | Free NPC | SnNPC |
|---|-------|-------|-------|----------|-------|
| λ_{\max} (nm) | 789 | 823 | 848 | 860 | 918 |
| ϵ (10 ⁴ M ⁻¹ cm ⁻¹) | 9.75 | 10.8 | 9.05 | 12.8 | 5.98 |

The UV-Visible spectra of free NPC were measured in several solvents, showing the maximum absorption variation in the ranges of 845 and 860 nm (Figure 1(a)). Compared with acetonitrile and methanol, the maximum absorption in toluene was red-shifted by 15 nm. Based on the solvent used, the red-shift of the Q-band increased in the order of acetonitrile < MeOH < THF < DMF < MIBK < toluene. The observations coincide with the previous results indicating that the red-shift of the Q-band increased linearly with the refractive index of solvent.¹⁹⁻²²

According to UV-Vis spectra of prepared MNPCs, the Q-band located well above 780 nm (Figure 1(b)). The Q-band of NPCs was heavily affected by the central metals, revealing that the absorption wavelength can be finely tuned between 780-920 nm. Compared to the free NPC, ruthenium (Ru), zinc (Zn), and nickel (Ni) showed a blue shift, while tin (Sn) induced a red shift. Maximum absorption wavelength and molar extinction coefficient values of MNPCs are summarized in Table 2.

The energy bandgap and molecular orbital diagrams and HOMO and lowest unoccupied molecular orbital (LUMO) levels of MNPCs were obtained by density functional theory (DFT) calculations. By doing this, it was intended to compare the contributions of the *d*-orbital electrons on the frontier molecular orbitals, and subsequently, to evaluate the motif for the change in Q-bands from the different central metals. First,

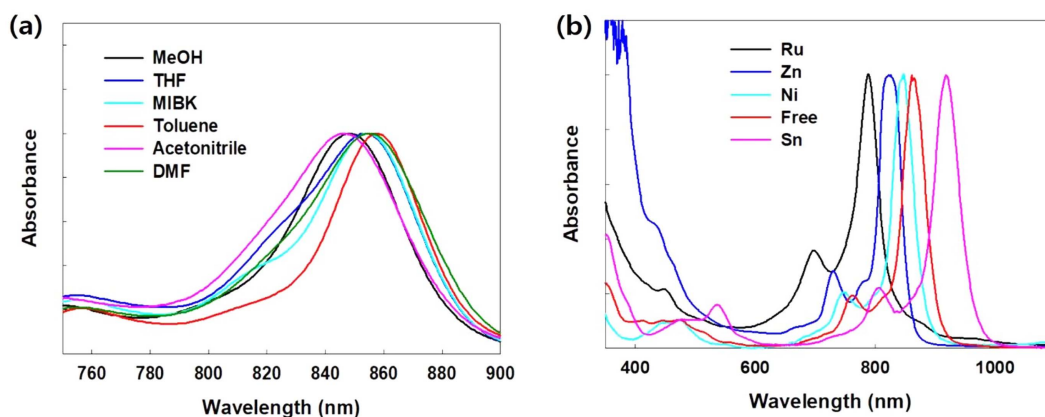


Figure 1. (a) UV-Vis absorption spectra of free NPCs in various solvents; (b) UV-Vis absorption spectra of various MNPC in DCM.

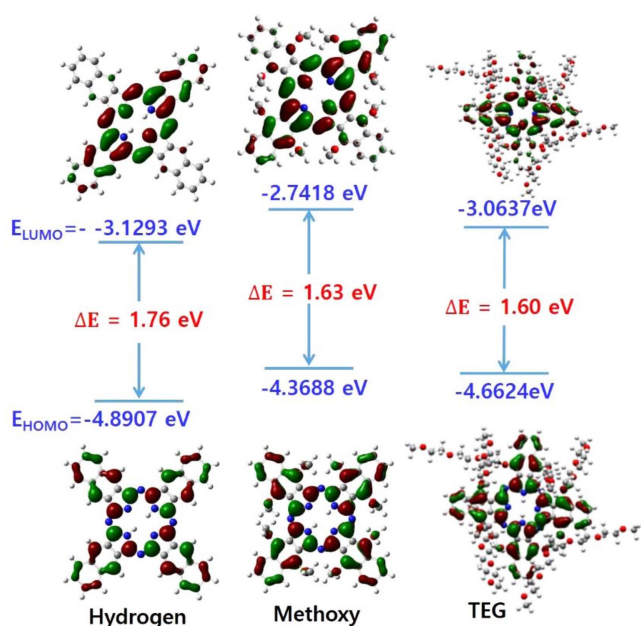


Figure 2. Molecular orbital distribution for free NPs with different substituents at α -positions.

we obtained the molecular orbitals of free NPc with three substituents of hydrogen, methoxy, and TEG groups (Figure 2). Without any substituents at α -position, the HOMO level is sta-

bilized, and the bandgap is 1.76 eV. The TEG introduction in the α -position destabilized the HOMO level, and the resulting bandgap became smaller than hydrogen substitution. In comparing the HOMO and LUMO levels of methoxy and TEG cases, an extended TEG substituent stabilized both HOMO and LUMO than those of the methoxy group. Compared to the hydrogen, the bandgaps of methoxy and TEG substitution were estimated to be reduced to 1.63 and 1.60 eV, respectively.

DFT calculations of MNPs having various central metals were also carried out (Figure 3). From the above observation, the methoxy substituent was applied in place of TEG in order to reduce the computation cost. The tin-naphthalocyanine, SnNPc, possessed a maximum absorption at a longer wavelength than free NPc. This red shift is attributed to the presence of p -block element at the center position, leading to stabilizing the LUMO level of SnNPc. Both LUMO (-3.39 eV) and HOMO (-4.89 eV) were stabilized with SnNPc, compared to those of free NPc (-2.74 and -4.36 eV, respectively). But, LUMO stabilization occurred more effectively, causing a smaller bandgap and resulting red-shift in Q-band absorption. Zn- and NiNPc showed insignificant differences in frontier orbital distribution and bandgap energy compared to free NPc. On the other hand, RuNPc showed an enlarged bandgap and

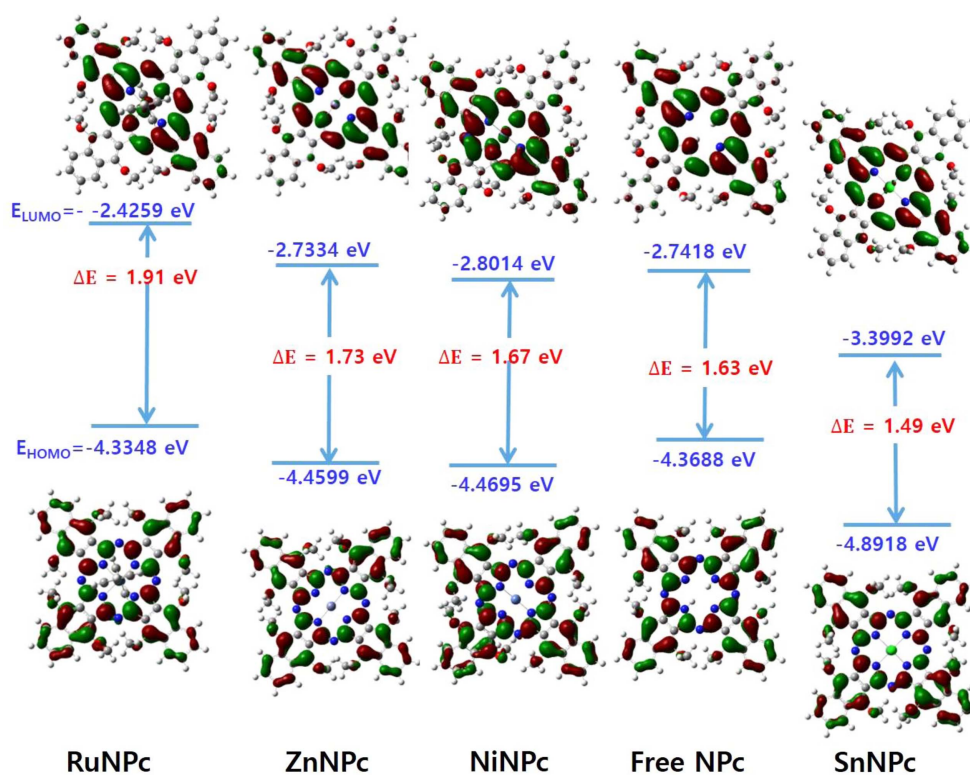
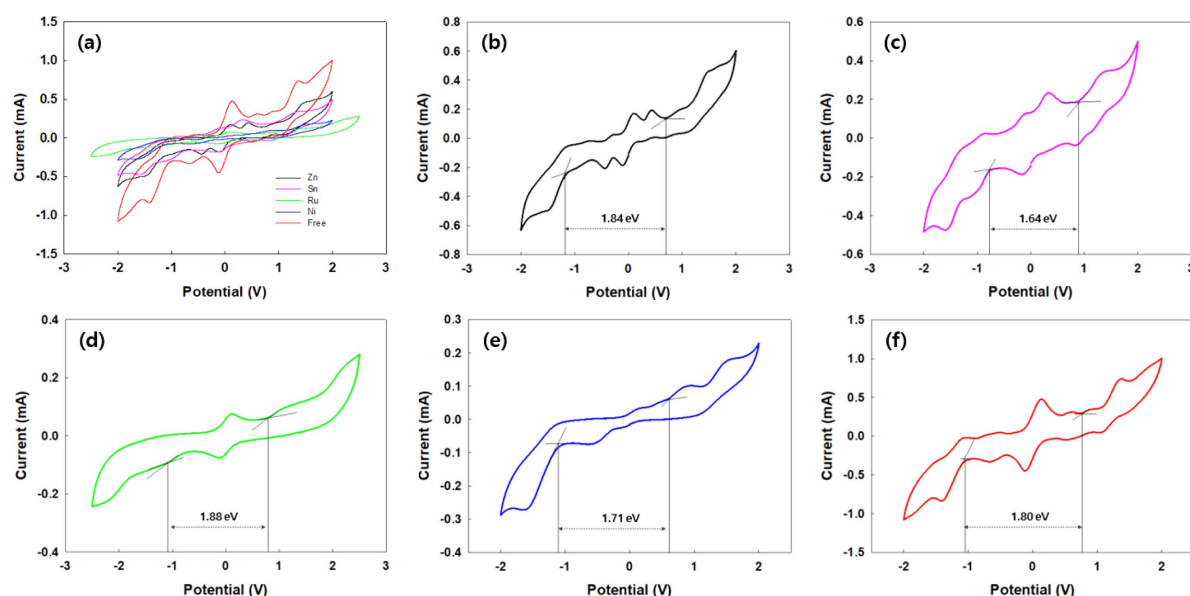


Figure 3. Molecular orbital distribution of various NPcs, containing different central metals.

Table 2. Comparison of Experimental and Calculated Bandgap and Absorption Maxima from UV-vis Spectra and DFT Studies, Respectively

| MNPc | Experimental wavelength (nm) | Experimental band gap (eV) | LUMO (eV) | HOMO (eV) | MO Energies (eV) | Calculated wavelength (nm) |
|----------|------------------------------|----------------------------|-----------|-----------|------------------|----------------------------|
| RuNPc | 789 | 1.57 | -4.33 | -2.43 | 1.90 | 652 |
| ZnNPc | 823 | 1.51 | -4.46 | -2.73 | 1.73 | 718 |
| NiNPc | 848 | 1.46 | -4.47 | -2.80 | 1.67 | 743 |
| Free NPc | 860 | 1.44 | -4.37 | -2.74 | 1.63 | 762 |
| SnNPc | 918 | 1.35 | -4.89 | -3.39 | 1.50 | 826 |

**Figure 4.** CV curves of MNPc ion gel containing electrochemical cells at the fixed scan rate of 100 mV/s: (a) combined; (b) ZnNPc (black); (c) SnNPc (pink); (d) RuNPc (green); (e) NiNPc (blue); (f) H2NPc (red).

blue-shifted absorption maximum than that of free NPc, which was originated from the strong destabilization of LUMO (-2.42 eV). The frontier molecular orbital levels, along with theoretically calculated and experimentally determined potential differences, are summarized in Table 2.

The electrochemical properties of MNPcs were evaluated by CV measurements using ion gel containing MNPcs (Figure 4).

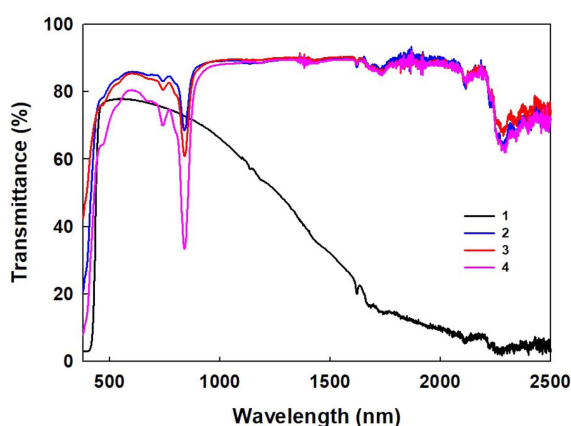
From the oxidation and reduction onsets of MNPcs, the HOMO and LUMO energy levels were estimated in the range of -5.66 to -5.39 eV and -4.02 to -3.62 eV, respectively. From these, the electrochemical bandgap energies were obtained around 1.64 to 1.88 eV. Electrochemical measurements confirmed the influence of the central metals. The detailed electrochemical data are summarized in Table 3. During CV

Table 3. Summarized Electrochemical Data of MNPc Based Electrochemical Cells

| MNPc | E_{ox} (V) | $E_{oxi,onset}$ (V) | HOMO (eV) | E_{red} (V) | $E_{red,onset}$ (V) | LUMO (eV) | E_g^{cc} (eV) |
|----------|--------------|---------------------|-----------|---------------|---------------------|-----------|-----------------|
| RuNPc | 1.07 | 0.78 | -5.58 | -1.07 | -1.10 | -3.70 | 1.88 |
| ZnNPc | 0.98 | 0.66 | -5.46 | -1.45 | -1.18 | -3.62 | 1.84 |
| NiNPc | 0.93 | 0.59 | -5.39 | -1.60 | -1.12 | -3.68 | 1.71 |
| Free NPc | 0.90 | 0.70 | -5.50 | -1.38 | -1.10 | -3.70 | 1.80 |
| SnNPc | 1.38 | 0.86 | -5.66 | -1.02 | -0.78 | -4.02 | 1.64 |

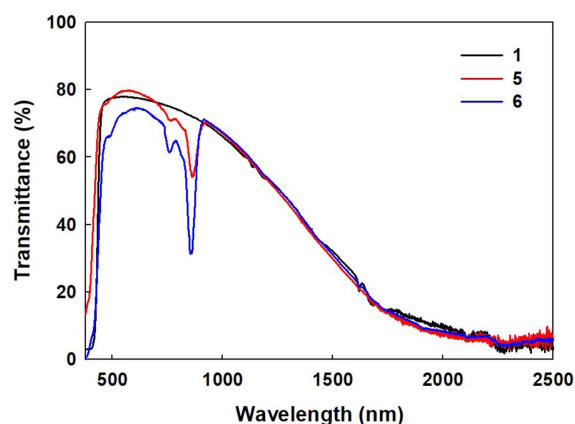
Table 4. The Compositions for the Preparation of NIR Blocking Films

| Composition | Resin (wt%) | ATO soln. (wt%) | NiNPc soln. (wt%) | IRC (%) | VLT (%) |
|-------------|-------------|-----------------|-------------------|---------|---------|
| 1 | 99 | 1 | - | 47.12 | 77.52 |
| 2 | 98 | - | 2 | 13.88 | 85.25 |
| 3 | 96 | - | 4 | 14.79 | 84.18 |
| 4 | 92 | - | 8 | 19.65 | 78.01 |
| 5 | 95.1 | 0.9 | 4 | 60.77 | 78.13 |
| 6 | 91.1 | 0.9 | 8 | 52.44 | 72.99 |

**Figure 5.** Transmittance curves of ATO-containing (**1**) and various amounts of NiNPc containing NIR blocking films (**2**, **3**, and **4**).

experiments, irreversible transitions were observed, accompanied by a slight color change in all MNPCs, mainly due to electron-rich characteristics of NPc fused rings.

High transmittance of NiNPc in the visible region can be taken advantage of for NIR blocking applications (Figure 5). For this purpose, various compositions for the NIR blocking films were prepared. After measuring the transmittance in the range of 380–2500 nm, the NIR cut-off (IRC) and visible light transmittance (VLT) values were calculated according to the KS-L2514 standard. The ATO coated film (**1**), similar to a commercialized blocking film, showed very low transmittance in the 1500–2500 nm and relatively high transmittance in the 780–1500 nm. VLT and IRC values were calculated as 77.52% and 47.12%, respectively. NiNPc coated film also had a very high VLT value of up to 85% (**2** and **3**). When 8 wt% of NiNPc was added (**4**), the VLT showed higher than 78%, and a sharp peak is formed at 850 nm. As the portion of the NiNPc solution increased, the transmittance in the visible region gradually decreases (**4**). As NiNPc was further increased, apparent

**Figure 6.** Transmittance curves of ATO (**1**) and NiNPc-ATO hybrid films (**5** and **6**).

aggregation with the photocurable resin occurs, causing a severe decrease in the visible transmittance. Films **2**, **3**, and **4** showed low blockage over 1000 nm, and thus the IRC values were less than 20%, significantly lower than film **1**.

The above observation showed that NiNPc and ATO have distinctive absorption below and above, respectively, 1000 nm. NiNPc-ATO hybrid films were prepared by utilizing the individual absorption behaviors, by which it was intended to provide efficient NIR blocking performances (Figure 6). The hybrid film exhibited significant changes in transmittance at 850 nm as the amount of NiNPc increased. The IRC value of film **5** was estimated as 50.77%, with an increase of 3.65% compared to pristine ATO film **1**. The VLT value also showed a small but slight increase to 78.13%. It is worthwhile to mention that NiNPc-ATO hybrid film exhibited a significant improvement of NIR-blocking performance without damaging the visible transmittance. However, by further increasing the

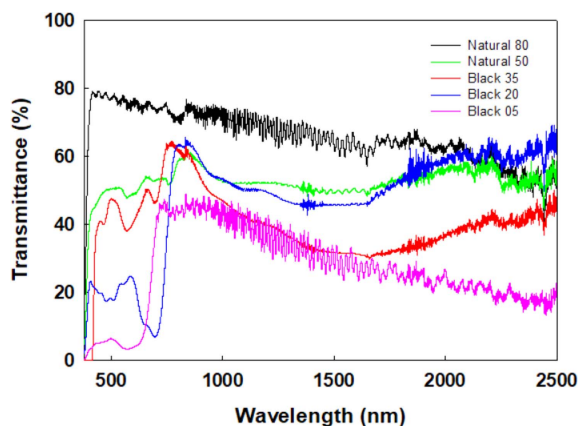
**Figure 7.** Transmittance curves of five commercially available NIR cut-off films.

Table 5. The IRC and VLT Values of five Commercially Available NIR Cut-off Films

| NIR cut-off films | (unit : %) | |
|-------------------|------------|-------|
| | IRC | VLT |
| Natural 80 | 32.01 | 76.38 |
| Natural 50 | 45.76 | 49.77 |
| Black 35 | 54.48 | 42.64 |
| Black 20 | 45.64 | 20.97 |
| Black 05 | 62.54 | 4.71 |

amount of NiNPc, film 6 showed an IRC increase to 52.44% but was accompanied by a significant VLT decrease to 72.99%. Reduced transmittance in the visible region is attributed to the aggregation of NiNPc. The compositions used for the NIR blocking films and resulting VLT and IRC values were summarized in Table 4.

The transmittance curves of five commercially available NIR cut-off films were measured for comparison purposes (Figure 7). The IRC values are between 32.01 and 62.54%, while the VLT values range from 76.38 to 4.71%, indicating the inversely proportional relationship between IRC and VLT values (Table 5). These results confirmed that the approach using NiNPc proves an excellent method for simultaneously obtaining NIR blocking ability and visible light transmittance.

Conclusion

MNPs substituted with TEG at the non-peripheral position showed a sharp Q-band absorption in the NIR and high transmittance in the visible regions. The absorption maxima can be finely tuned in the range of 780-920 nm depending on the central metal ion. Electrochemical studies revealed that the influence of the central metal ion on the HOMO and LUMO stabilization. NiNPc-ATO hybrid films were prepared by mixing NiNPc and ATO to utilize distinctive absorption ranges below and above, respectively, 1000 nm. The NIR blocking performance was improved by 3.65% while maintaining the identical visible transmittance. Current results demonstrate that MNPs can be effectively employed as a NIR blocking material that is applied for useful applications, including solar glasses and NIR electronic shutters.

Acknowledgments: This work was supported by the Technology Innovation Program (20011133 and 20010034) funded by the Ministry of Trade, Industry, and Energy (MOTIE, Korea).

References

1. Nguyen, T. K. N.; Renaud, A.; Wilmet, M.; Dumait, N.; Paofai, S.; Dierre, B.; Chen, W.; Ohashi, N.; Cordier, S.; Grasset, F.; Uchikoshi, T. New Ultra-Violet and Near-infrared Blocking Filters for Energy Saving Applications: Fabrication of Tantalum Metal Atom Cluster-Based Nanocomposite Thin Films by Electrophoretic Deposition. *J. Mater. Chem. C* **2017**, *5*, 10477-10484.
2. Medina, I.; Newton, E.; Kearney, M. R.; Mulder, R. A.; Porter, W. P.; Stuart-Fox, D. Reflection of Near-infrared Light Confers Thermal Protection in Birds. *Nat. Commun.* **2018**, *9*, 3610.
3. Lamnatou, C.; Chemisana, D. Solar Radiation Manipulations and Their Role in Greenhouse Claddings: Fresnel Lenses, NIR- and UV-Blocking Materials. *Renew. Sust. Energy. Rev.* **2013**, *18*, 271-287.
4. Xu, X.; Zhang, W.; Hu, Y.; Wang, Y.; Lu, L.; Wang, S. Preparation and Overall Energy Performance Assessment of Wide Waveband Two-Component Transparent NIR Shielding Coatings. *Sol. Energy Mater. Sol. Cells* **2017**, *168*, 119-129.
5. Yao, Y.; Zhang, L.; Chen, Z.; Cao, C.; Gao, Y.; Luo, H. Synthesis of Cs₂WO₆ Nanoparticles and Their NIR Shielding Properties. *Ceram. Int.* **2018**, *44*, 13469-13475.
6. Abendroth, T.; Schumm, B.; Alajlan, S. A.; Almogbel, A. M.; Mäder, G.; Härtel, P.; Althues, H.; Kaskel, S. Optical and Thermal Properties of Transparent Infrared Blocking Antimony Doped Tin Oxide Thin Films. *Thin Solid Films* **2017**, *624*, 152-159.
7. Xingyu, X.; Lin, L. Antimony Doped tin Oxide/Multi-walled Carbon Nanotubes: Highly Near-infrared Blocking Coating used for Heat Conservation Windows. *Energy Procedia* **2017**, *105*, 4836-4841.
8. Fang, D.; Yu, H.; Dirican, M.; Tian, Y.; Xie, J.; Jia, D.; Yan, C.; Liu, Y.; Li, C.; Liu, H.; Wang, J.; Tang, F.; Chen, G.; Zhang, X.; Tao, J. Disintegrable, Transparent and Mechanically Robust High-Performance Antimony Tin Oxide/Nanocellulose/Polyvinyl Alcohol Thermal Insulation Films. *Carbohydr. Polym.* **2021**, *266*, 118175.
9. Krishnakumar, T.; Jayaprakash, R.; Pinna, N.; Phani, A.; Passacantando, M.; Santucci, S. Structural, Optical and Electrical Characterization of Antimony-Substituted Tin Oxide Nanoparticles. *J. Phys. Chem. Solids* **2009**, *70*, 993-999.
10. Gould, R. Structure and Electrical Conduction Properties of Phthalocyanine Thin Films. *Coord. Chem. Rev.* **1996**, *156*, 237-274.
11. Son, H.; Ji, J. H.; Jeong, J. H.; Han, S. H.; Koh, J. H.; Park, J. S. Noncovalent Functionalization of Single-walled Carbon Nanotubes Using Alkylated Zinc-phthalocyanine for the β -phase Formation of a Polyvinylidene Fluoride Matrix. *Polym. Korea* **2020**, *44*, 301-308.
12. Son, H. S.; Yang, M. H.; Mutyala, A. K.; Chang, D. W.; Park, J. S. Superior Electrocatalytic Performance of Polyisobutylene-substituted Metallophthalocyanines Supported on Single-Walled Carbon Nanotubes for an Oxygen Reduction Reaction. *Dyes*

- Pigm.* **2019**, 162, 662-670.
- van Leeuwen, M.; Beeby, A.; Fernandes, I.; Ashworth, S. H. The Photochemistry and Photophysics of a Series of Alpha Octa(alkyl-substituted) Silicon, Zinc and Palladium Phthalocyanines. *Photochem. Photobiol. Sci.* **2014**, 13, 62-69.
 - Sakamoto, K.; Ohno-Okumura, E.; Kato, T.; Soga, H. Synthesis of Near-infrared Absorbed Metal Phthalocyanine with S-Aryl Groups at Non-Peripheral Positions. *J. Porphyr. Phthalocya.* **2010**, 14, 47-54.
 - Hirao, A.; Akiyama, T.; Okujima, T.; Yamada, H.; Uno, H.; Sakai, Y.; Aramaki, S.; Ono, N. Soluble Precursors of 2,3-Naphthalocyanine and Phthalocyanine for Use in Thin Film Transistors. *Chem. Commun.* **2008**, 4714-4716.
 - Rawling, T.; McDonagh, A. Ruthenium Phthalocyanine and Naphthalocyanine Complexes: Synthesis, Properties and Applications. *Coord. Chem. Rev.* **2007**, 251, 1128-1157.
 - Taratula, O.; Schumann, C.; Duong, T.; Taylor, K. L.; Taratula, O. Dendrimer-Encapsulated Naphthalocyanine as a Single Agent-Based Theranostic Nanoplatfrom for Near-Infrared Fluorescence Imaging and Combinatorial Anticancer Phototherapy. *Nanoscale* **2015**, 7, 3888-3902.
 - Choi, M. T.; Li, P. P.; Ng, D. K. A Direct Comparison of the Aggregation Behavior of Phthalocyanines and 2,3-Naphthalocyanines. *Tetrahedron* **2000**, 56, 3881-3887.
 - Batat, P.; Bayar, M.; Pur, B.; Çoker, E.; Ahsen, V.; Yuksel, F.; Demirel, A. L. The Optical Characterization of Metal-Mediated Aggregation Behaviour of Amphiphilic Zn(II) Phthalocyanines. *Phys. Chem. Chem. Phys.* **2016**, 18, 15574-15583.
 - Hiroaki, I.; Yutaka, K.; Akiyuki, M. Solvatochromic Shift of Phthalocyanine Q-band Governed by a Single Solvent Parameter. *Chem. Lett.* **2004**, 33, 862-863.
 - Kudrik, E. V.; Afanasiev, P.; Bouchu, D.; Sorokin, A. B. Solvent-Dependent Rotational Phenomena in μ -Nitrido-[2,3,9,10,16,17,23,24-octa(n-pentoxy)phthalocyaninato]diiron Complex. *J. Porphyr. Phthalocya.* **2011**, 15, 583-591.
 - Kang, I. S.; Lee, T. J.; Seo, M. J.; Hwang, S. Y.; Park, N. K.; Lee, S. W. Preparation and Characterization of Absorbent Materials on Glass-Web Fibers for Removal of Mercury Ion. *Polym.-Korea* **2019**, 43, 793-797.

Publisher's Note The Polymer Society of Korea remains neutral with regard to jurisdictional claims in published articles and institutional affiliations.